Optimization of Nanocomposite Materials for Permanent Magnets: Micromagnetic Simulations of the Effects of Intergrain Exchange and the Shapes of Hard Grains

Sergey Erokhin and Dmitry Berkov*

General Numerics Research Lab, Moritz-von-Rohr-Strasse 1A, D-07749 Jena, Germany

(Received 22 August 2016; revised manuscript received 7 November 2016; published 17 January 2017)

In this paper, we perform a detailed numerical analysis of remagnetization processes in nanocomposite magnetic materials consisting of magnetically hard grains (i.e., grains made of a material with a high magnetocrystalline anisotropy) embedded into a magnetically soft phase. Such materials are widely used for the production of permanent magnets because they combine high remanence with large coercivity. We perform simulations of nanocomposites with Sr-ferrite as the hard phase and Fe or Ni as the soft phase, concentrating our efforts on analyzing the effects of (i) the imperfect intergrain exchange and (ii) the nonspherical shape of hard grains. We demonstrate that—in contrast to common belief—the maximal energy product is achieved not for systems with a perfect intergrain exchange, but for materials where this exchange is substantially weakened. We also show that the main parameters of the hysteresis loop—remanence, coercivity, and the energy product—exhibit nontrivial dependencies on the shape of hard grains and provide detailed explanations for our results. Simulation predictions obtained in this work open new ways for the optimization of materials for permanent magnets.

DOI: 10.1103/PhysRevApplied.7.014011

I. INTRODUCTION

Magnetic materials which can be used for the manufacturing of permanent magnets are among the key materials used in many high-technology applications today [1]. Modern electromotors, actuators, and magnetic-field-based sensors (to name only a few applications) require high-performance magnets. The effectiveness of these magnets is usually estimated by the value of the maximal energy product $(BH)_{\max}$ achieved in the second quadrant of their B-H hysteresis loop. One of the most promising ways to obtain large values of this parameter is the usage of magnetic nanocomposites, i.e., materials which combine a high coercivity of a magnetically hard phase (the phase made of a material possessing a large magnetocrystalline anisotropy) with the high saturation magnetization of another (soft) phase.

At present, the best performance magnets are produced from rare-earth metals (NdFeB, SmCo) and by employing the precise fabrication control (see, e.g., Ref. [2]). Unfortunately, these magnets are relatively expensive and are subject to availability and price fluctuations due to the high volatility of the rare-earth-element market.

Another very important class of materials for permanent magnets is represented by nanocomposites containing ferrites as the hard phase. The energy product of Co-, Ba-, and Sr-ferrite-based magnets is sufficient for many applications of permanent magnets, e.g., in microwave devices, telecommunication, recording media, and electronic industry. Another important advantage of these materials is that they have a much better temperature and corrosion resistance than NdFeB-based magnets (see, e.g., Chap. 12.2 in Ref. [3]). In addition, the situation with the production of ferrite-based magnets is more stable, and costs are much lower due to the wider availability of the corresponding raw materials.

The specified performance of a nanocomposite material can, in principle, be achieved by tailoring various parameters of a nanocomposite, such as relative fractions of the soft and hard phases, the size and shape of hard grains, mutual arrangement of grains belonging to different phases, and the quality of the intergrain boundaries. The development of new magnets of any type requires a thorough understanding of the relationship between their microstructure and their magnetic properties [4]. Advanced structural experimental techniques can provide a very important information; well-known examples are, e.g., the electron Bragg scattering diffraction studies of the grain alignment in sintered NdFeB [5] or the x-ray diffraction along with the high-resolution transmission electron microscopy applied for the measurements of the grain size distribution in soft magnetic alloys [6].

Recent publications of different scientific collaborations have shown that, in order to study the question of the microstructure-magnetism relationship in detail, it is absolutely necessary to employ numerical modeling—in particular, micromagnetic simulations—combining it with other experimental methods like 3D atom probe [7], energy-dispersive x-ray spectroscopy [8], and magnetic neutron scattering [9,10]. The use of micromagnetic modeling in the development process allows the *a priori* performance optimization of permanent magnets by predicting magnetic characteristics of a nanocomposite material before its actual manufacturing.

*d.berkov@general-numerics-rl.de

In general, micromagnetic simulations are perfectly suited for modeling of magnetic composites because the typical micromagnetic length—a few nanometers—allows us to resolve very well the magnetization distribution inside the nanocomposite grains with sizes of several tens of nanometers. However, corresponding simulations require an enormous computational effort, for two main reasons. First, a very fine mesh of finite elements is required for the adequate approximation of each single grain as a geometrical object with a complicated shape. Second, a large number of soft and (especially) hard grains should be present in the simulated volume, in order to study the magnetization reversal as a collective phenomenon and to obtain a sufficiently accurate statistics for these disordered systems (see a detailed discussion of these issues in Refs. [11–13]).

In recent years, a major simulation effort was devoted to the understanding of rare-earth-based materials, with the strategic goal to "push the border" of the conventional (nonsuperconducting) magnets. In the first line, a large amount of numerical research was carried out for composites based on NdFeB [7,8,14–16] and PrFeB [17–19]; some results have also been published for SmCo and similar compounds [20].

For NdFeB-based materials, the question of internal magnetization structure (mainly vortex) in a single grain have been studied [14]. The influence of the soft-phase concentration (Fe or FeB), the hard-grain size [15] and (very recently) magnetic behavior of hard grains for several different shapes [16] was investigated. Special attention was paid to Nd-rich compositions, where it has been shown that enrichment with Nd leads to coercivity enhancement due to the concentration of the additional Nd on intergrain boundaries [7,8].

Studies of composites based on PrFeB and containing Fe as the soft phase have been devoted to the increasing role of the magnetodipolar interaction with the growing soft-phase fraction [17], correlation of the magnetization reversal of the soft and hard grains [18], and the effect of the hard-grain alignment [19]. For SmCo-like materials, different mechanisms of the magnetization reversal when changing the angle between the anisotropy axis and the applied field were identified [20].

Somewhat apart from the main path lie the simulations of a highly interesting yet not really applicable class of MnBi-based materials. Here, the influence of the soft-phase concentration (Co and FeCo) and the orientation degree of the hard-grain anisotropy axes was studied numerically in Ref. [21].

In contrast to the rare-earth-based composites, materials based on various ferrites as the hard phase have not been studied—to our knowledge—by micromagnetic simulations, although this class of materials becomes increasingly important for the reasons listed above. In this paper, we address this challenge, starting with detailed studies of the effect of the intergrain exchange coupling and the influence of the hard-grain shape on the material properties in nanocomposites $SrFe_{12}O_{19}$/Fe and $SrFe_{12}O_{19}$/Ni.

Our polyhedron-based micromagnetic algorithm provides a high statistical accuracy of simulated results because we are able to handle systems containing a few thousand grains, including the ability to resolve a possibly nontrivial magnetization distribution in every grain. Because of the flexibility of our mesh-generation method, a nearly arbitrary grain shape can be adequately approximated so that a simulated sample may include the grains of different shapes and sizes.

The paper is organized as follows. In Sec. II, we explain the mesh-generation methods which we use to create a polyhedron mesh for a system containing nonspherical hard grains embedded in a magnetically soft matrix; micromagnetic energy contributions and their evaluation in our methodology are also briefly presented. Section III contains simulation results. Section III A is devoted to a detailed analysis of the influence of the intergrain exchange weakening on the magnetization reversal in our materials. The main result there is that the maximal energy product is achieved for an intergrain exchange coupling that is much smaller than the perfect coupling. Section III B deals with the effect of the nonspherical shapes of the hard grains, which turns out to be highly nontrivial and has a very interesting underlying physical mechanism. Both subsections contain a detailed physical discussion of the results obtained. We conclude with a summary of our findings and offer possible perspectives for the improvement of ferrite-based composites in Sec. IV.

II. OUR MICROMAGNETIC METHODOLOGY FOR SIMULATION OF NANOCOMPOSITES

To overcome the difficulties in modeling magnetic nanocomposites using standard micromagnetic methods (finite difference and tetrahedral finite elements), we develop [13] an alternative micromagnetic methodology based on a discretization of magnetic materials using polyhedrons of a special type. This methodology combines the flexibility of general finite-element schemes for the geometrical description of a nanocomposite structure with the possibility of using fast Fourier transformation for the calculation of the most time-consuming contribution to the total energy: the magnetodipolar interaction.

A. Mesh generation for grains of a general shape

One of the main questions discussed in this paper is the influence of the nonspherical (spheroidal) shape of hard grains on the magnetic behavior of nanocomposites. For such a system, we have to introduce two additional steps into the mesh-generation procedure described in our previous publications [11–13]. Namely, in this work, the mesh for hard grains is generated separately from the

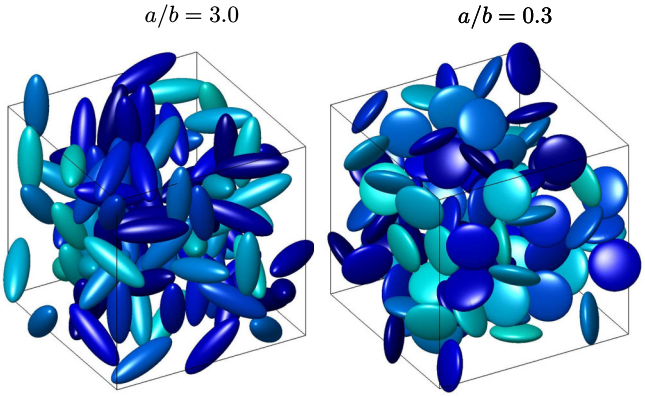

FIG. 1. Examples of a spatial distribution of hard crystallites (soft crystallites are not shown) in simulated samples for different aspect ratios a/b of corresponding ellipsoids of revolution (see the text for details).

soft-phase mesh (Fig. 1; additional step 1) and the two systems are then merged (Fig. 2; additional step 2).

As in our standard methodology, we start from the generation of mesh consisting of small, nearly spherical polyhedrons with sizes less than the characteristic micromagnetic length. These polyhedrons will be used in micromagnetic simulations as the corresponding finite elements (see Refs. [11–13] for details).

Next, we generate a system of nonoverlapping ellipsoidal particles (additional step 1) with sizes and shapes corresponding to the hard grains of our composite. We point out that the generation of an ensemble of nonoverlapping ellipsoids is computationally challenging: the evaluation of an overlapping of two ellipsoids and the introduction of the suitable overlapping criterion require a development of a special numerical scheme. We use a method described by Donev *et al.* [22], which is based on the Perram-Wertheim overlap potential and

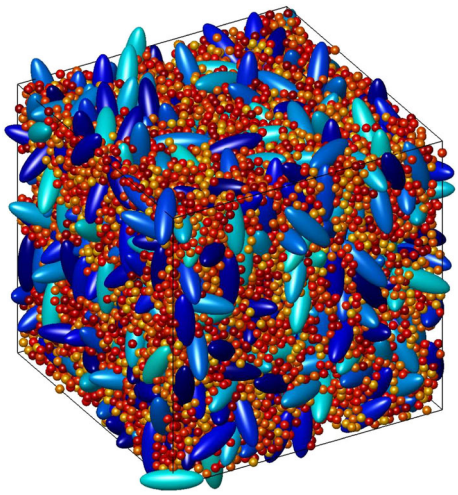

FIG. 2. Example of a microstructure (hard and soft phases) used in our modeling of nanocomposites.

provides a suitable parameter describing the overlapping degree of two ellipsoids. This parameter is then used in a model of interacting particles with a short-range repulsive potential, where ellipsoids are initially placed randomly, but, due to the nature of this potential, the number of overlaps is continuously decreasing.

At the second additional step, these ellipsoids are mapped onto the system of (much smaller) polyhedrons used as mesh elements in our micromagnetic simulation. By this mapping, all mesh elements with centers inside ellipsoids are assigned to the hard phase, and the rest of elements to the soft phase. Note that the discretization of crystallites of the soft and hard phases is based on mesh elements of the same size.

All mesh elements belonging to the same spheroid (crystal grain) have the same direction of the magnetocrystalline anisotropy axes. We note here also that anisotropy axis directions assigned to "soft" grains (Fe and Ni, in our system), which are approximately spherical, are distributed randomly in space; it should also be mentioned that, for the soft phase, both the anisotropy-axis distributions and the exact values of the anisotropy constants play a minor role compared to the influence of other interactions. For a spheroidal (ellipsoid of revolution) "hard" grain, the anisotropy-axis direction coincides with its rotational-symmetry axis.

B. Energy contributions and minimization procedure

In our simulations, we take into account all four standard contributions to the total magnetic free energy: energy in the external field, magnetocrystalline-anisotropy energy, exchange stiffness, and magnetodipolar-interaction energies [11–13].

The energy in the external field and the magnetocrystalline-anisotropy energy are computed in a standard way, by multiplying the corresponding energy densities by the volume of finite elements (polyhedrons, in our case) and summing over all of these elements. Evaluation of the exchange energy is discussed in detail in Sec. III A. The magnetodipolar field and energy are computed using an optimized version of the lattice Ewald method for disordered systems. In this algorithm, the mapping of the initial (disordered) system of mesh elements on the translationally invariant regular lattice allows us to keep the high speed of the lattice method (fast Fourier transformation), while at the same time making the mapping errors negligibly small. We point out that a mapping of our disordered grid to the regular lattice is necessary only for the fast evaluation of the magnetodipolar interaction via FFT; all other micromagnetic interactions are computed directly using the disordered mesh.

For a minimization of the total magnetic energy, obtained as the sum of all four contributions described above, we use a simplified version of a gradient method employing the dissipation part of the Landau-Lifshitz equation of motion

for magnetic moments [23,24]. The minimization is considered converged when the condition for the local torque $\max_{\{i\}}|[\mathbf{m}_i \times \mathbf{h}_i^{\text{eff}}]| < \varepsilon$ is fulfilled (here, $\mathbf{m}_i$ is a normalized magnetic moment of the ith mesh element and $\mathbf{h}_i^{\text{eff}}$ is the corresponding effective field; the value $\varepsilon = 10^{-3}$ is found to be small enough for our quasistatic minimization procedure).

Further details of our method can be found in Ref. [13].

III. RESULTS AND DISCUSSION

Because of the high performance of our methodology, we are able to simulate bulk nanocomposites with hard grains of any prescribed shape, whereby the simulated system may contain up to 600 hard grains, with an average discretization of 300 mesh elements per grain. The whole simulation volume is a cube with sides 220 nm long and is discretized into finite elements (polyhedrons) that approximately equal 4×10^5. Employing this algorithm, we could obtain systematic results with a high statistical accuracy for two model systems: $SrFe_{12}O_{19}$/Fe and $SrFe_{12}O_{19}$/Ni. Every data point in the figures presented below is the result of averaging over four independent simulation runs, each with a new random configuration of soft and hard grains.

For simulations of these nanocomposites, we use standard magnetic parameters of the corresponding materials (see, e.g., Ref. [3], Chaps. 5.3 and 11.6), which are summarized in Table I.

The average grain volume for all phases is chosen to be equal to the volume of a spherical grain with the diameter $D = 25$ nm. The volume concentration of the hard phase in all presented simulations is $c_{\text{hard}} = 40\%$.

A. Effect of the exchange weakening in $SrFe_{12}O_{19}$/Fe

One of the central questions for permanent magnets made of nanocomposite materials is the dependence of magnetic properties on the exchange weakening between different grains. This weakening is unavoidable in real systems because it is nearly impossible to obtain perfect intergrain boundaries. The quality of these boundaries strongly depends on the concrete method used for the manufacturing of a nanocomposite, and substantial efforts have been devoted to obtaining materials with more-perfect intergrain boundaries (and especially boundaries between grains belonging to different phases) in order to achieve better exchange coupling. However, recently [25], it was demonstrated both experimentally and theoretically that the perfect intergrain exchange may strongly decrease the performance of a magnetic nanocomposite material, so this possibility requires a detailed theoretical study.

TABLE I. Magnetic properties of various materials used in simulations.

	$SrFe_{12}O_{19}$	Fe	Ni
M_s (G)	400	1700	490
Anis. kind	uniaxial	cubic	cubic
K (erg/cm^3)	4.0×10^6	5.0×10^5	-4.5×10^4
A (erg/cm)	0.6×10^{-6}	2.0×10^{-6}	0.8×10^{-6}

The exchange energy in our methodology is computed in the nearest-neighbor (NN) approximation as

$$E_{\text{exch}} = -\frac{1}{2}\sum_{i=1}^{N}\sum_{j\subset \text{NN}(i)} \kappa_{ij}\frac{2A_{ij}\bar{V}_{ij}}{\Delta r_{ij}^2}(\mathbf{m}_i\mathbf{m}_j), \qquad (1)$$

where $\bar{V}_{ij} = (V_i + V_j)/2$, Δr_{ij} is the distance between the centers of the ith and jth finite elements, with volumes V_i and V_j. The exchange constant A_{ij} for the homogeneous bulk material is equal to the corresponding exchange stiffness constant A, but it is obviously site dependent in composite materials; detailed justification of expression (1) can be found in Refs. [12,13].

The exchange weakening is defined by multiplying the exchange energy of neighboring mesh elements in Eq. (1) by a factor $0 \le \kappa_{ij} \le 1$. As we study here the influence of the intergrain exchange weakening, $\kappa_{ij} = 1$ if the neighboring magnetic moments i and j are located in the same grain (crystallite). If neighboring moments belong to different grains, then κ_{ij} may be < 1 and is the same for all intergrain boundaries. From Eq. (1), it can be seen that $\kappa = 1$ corresponds to the perfect intergrain exchange (equal to the exchange within a bulk material), and $\kappa = 0$ indicates no exchange interaction at all between different grains.

Dependence of magnetic properties on this exchange weakening is studied for the composite $SrFe_{12}O_{19}$/Fe with approximately spherical hard grains (obtained from the random placement of spheres with $D = 25$ nm; see Sec. II A).

The overall trend is shown in Fig. 3, where the evolution of hysteresis curves by increasing the exchange coupling ($\kappa = 0.0 \to 0.5$) between grains is demonstrated. Systems without ($\kappa = 0.0$) or with a strongly reduced ($\kappa = 0.05$) exchange coupling between grains exhibit the two-step magnetization reversal. The first step—a large jump on the hysteresis loop in small negative fields (see the panel for $\kappa = 0.05$ in Fig. 3)—represents the magnetization reversal of the soft phase, whose volume fraction is relatively high. The second step—reversal of hard grains in much higher fields—leads to the closure of the loop. Reversal of the hard phase occurs in fields around H_K^{hard}, where the anisotropy field is defined as $H_K = 2K/M_s = \beta M_s$ ($\beta = 2K/M_s^2$ denotes the reduced anisotropy constant). The large magnitude of the magnetization jump during the first reversal step is due to the dominating contribution of the soft phase to the system magnetization: $m_{\text{soft}} = c_{\text{soft}}M_{\text{soft}}/(c_{\text{hard}}M_{\text{hard}} + c_{\text{soft}}M_{\text{soft}}) \approx 0.86$.

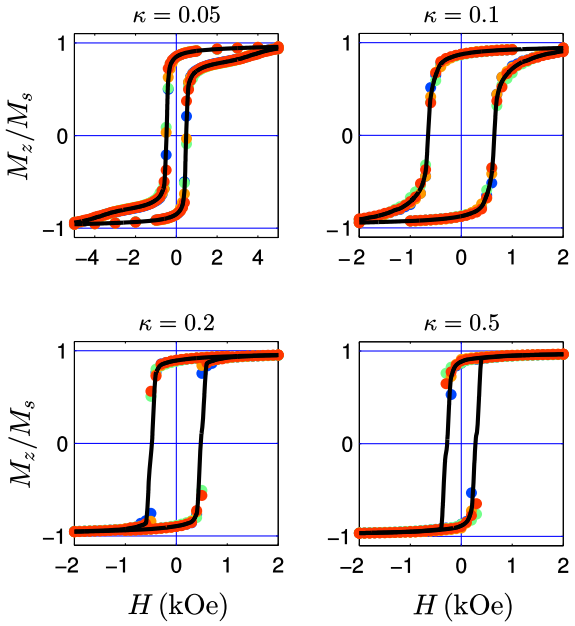

FIG. 3. Simulated hysteresis curves of the nanocomposite $SrFe_{12}O_{19}/Fe$ with spherical hard grains for different exchange-weakening constant.

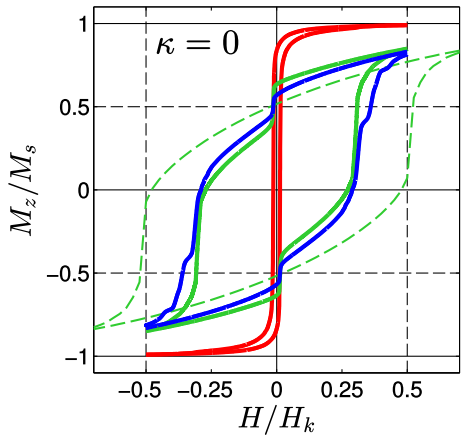

FIG. 4. Simulated hysteresis loops for $SrFe_{12}O_{19}/Fe$ (with spherical hard grains) without the intergrain exchange ($\kappa = 0$) presented for hard (solid blue line) and soft (solid red line) phases separately. The dashed line represents the unsheared loop of the SW model with particle parameters, as for $SrFe_{12}O_{19}$. The solid green line represents the SW loop sheared according the averaged internal field (see the text for details). The external field is normalized by the anisotropy field of the hard phase $H_K = \beta_h M_h = 20$ kOe.

For a detailed analysis of the magnetization reversal in a magnetic composite, it is very useful to plot hysteresis loops for the soft and hard phases separately. Such loops can be easily obtained from simulated magnetization configurations by summing up contributions from finite elements belonging to either the soft or the hard phase and calculating corresponding total magnetizations of these phases.

We begin our consideration from systems with an absent or very low intergrain exchange coupling, where the dominant interaction is the magnetodipolar one. To clarify the effect of this interaction, the above-mentioned magnetization-reversal curves of hard and soft phases are plotted in Fig. 4 for the composite without any intergrain exchange coupling ($\kappa = 0$).

In order to understand the hysteretic behavior of both phases, it is useful to calculate the reduced anisotropy constant $\beta = 2K/M_s^2$, whose magnitude gives (roughly speaking) the relation of the magnetocrystalline-anisotropy field to the magnetodipolar field from the nearest neighbor in the system of spherical particles. Substitution of the magnetic parameters of our materials (see Table I) results in the values $\beta_h = 50(\gg 1)$ for the hard phase ($SrFe_{12}O_{19}$) and $\beta_s = 0.34(\sim 1)$ for the soft phase (Fe). We note that the much higher value of β for the hard phase is due not only to its large anisotropy constant K (which is "only" 8 times larger than by Fe), but mainly due to the much higher value of the soft-phase magnetization $M_{Fe}/M_{SrFeO} = 4.25$, which gives an additional factor approximately equal to 18.

Considering the magnetization reversal of the *soft* phase first, we note that this phase would exhibit in the absence of the magnetodipolar interaction the "ideal" hysteresis loop for a system of noninteracting particles with the cubic anisotropy constant $K_{cub} > 0$ (as is the case with Fe). Such a loop has the remanence $j_R^{(0)} \approx 0.83$ and the coercivity $H_c^{(0)} \approx 0.33 H_K = 0.33\beta M_s \approx 195$ Oe (see, e.g., Ref. [26]). The relatively low value of the reduced anisotropy for our soft phase $\beta_s(\mathrm{Fe}) = 0.34$ means that the magnetodipolar interaction can considerably modify the corresponding ideal hysteresis. This influence manifests itself primarily in the smoothing of the ideal loop [26], as can be seen in Fig. 4, where the loop for the soft phase of our system is shown in red. The remanence $j_R \approx 0.836$ is nearly the same and the coercivity $H_c \approx 260$ Oe increases by approximately 30% compared to the noninteracting case.

Unfortunately, we are not aware of any systematic theoretical studies of the magnetodipolar-interaction effects in systems of "cubic" particles, except for Ref. [27], where only simulation results for the Henkel plots are shown; any quantitative comparison with a detailed study of these effects for the "uniaxial" particles presented in Ref. [28] is meaningless due to the very different energy landscapes for these two anisotropy types. For this reason, we can only suggest that the nearly unchanged remanence (compared to the ideal system) is due to the interplay of the magnetodipolar interactions within the soft phase and between the soft and hard phases. The increase of H_c is most probably due to the "supporting" action of the magnetodipolar field from the hard phase onto the soft grains. Magnetization of the hard phase in our system is rather low, so the corresponding effect is relatively small.

The noninteracting hard phase consisting of grains with the uniaxial anisotropy (as for $SrFe_{12}O_{19}$) would reverse

according to the ideal Stoner-Wohlfarth (SW) loop [29], with $j_R = 0.5$ and $H_c \approx 0.48 H_K \approx 10$ kOe indicated in Fig. 4 by a thin dashed green line. The very large value of the reduced single-grain anisotropy $\beta_h(\mathrm{SrFeO}) = 50$ for this phase indicates that intergrain correlations of hard-phase magnetic moments are negligible. However, in our composite material hard grains are "embedded" in the soft phase. Hence, in order to properly compare (at least in the mean-field approximation) the simulated hard-phase loop—the blue solid line in Fig. 4—to the SW model, we have to take into account the average magnetodipolar field $\langle H_{\mathrm{md},z} \rangle = (4\pi/3)\langle M_z^{\mathrm{soft}} \rangle$ acting on a spherical particle inside a continuous medium with the average magnetization of the soft phase $\langle M_z^{\mathrm{soft}} \rangle$.

Correction of the SW loop using this internal field [which depends on the external field via the corresponding dependence $\langle M_z(H_z) \rangle$] leads to the loop shown with the thick solid green line in Fig. 4. It can be seen that this corrected SW loop is in good agreement with the simulated hard-phase loop. The remaining discrepancies are due to local internal field fluctuations (always present in disordered magnetic systems), which are especially pronounced in our composite due to the high difference between the magnetizations of the soft and hard phases.

This analysis reveals that the first jump on the hard-phase loop in small negative fields is due to the abrupt change in the internal averaged dipolar field due to the magnetization reversal of the soft phase. The second jump—for $H_z/H_k \approx -0.3$—is the manifestation of the singular behavior of the SW loop of the hard phase itself, which occurs for the unsheared loop at $H_{\mathrm{cr}} = -H_k/2$ (near this field, $M_z \sim \sqrt{-(H_z - H_{\mathrm{cr}})}$ for $H_z < H_{\mathrm{cr}}$ [30]).

In summary, despite a relatively high saturation magnetization, $M_s = 1180$ G, the corresponding composite without any intergrain exchange coupling would have only a relatively small maximal energy product of approximately 15 kJ/m^3 [see Fig. 5(b)]. The reason is its very small coercivity $H_c \approx 250$ Oe, which is determined entirely by the magnetization reversal of the soft phase in small negative fields.

Before we proceed with an analysis of the effect of the intergrain exchange coupling on the hysteretic properties of a nanocomposite, an important methodical issue should be clarified. Namely, we have to determine the maximal value of the exchange coupling (the maximal value of κ), for which our simulations can produce meaningful results.

The problem is that, with an increase of the coupling strength, the interaction between the grains increases, so that grains start to form clusters, inside which magnetic moments of constituting grains reverse nearly coherently. The average size of such a cluster, $\langle d_{\mathrm{cl}} \rangle$, obviously grows with an increasing κ. In order to obtain statistically significant results, we have to assure that $\langle d_{\mathrm{cl}} \rangle$ is significantly less (ideally much less) than the maximal system size

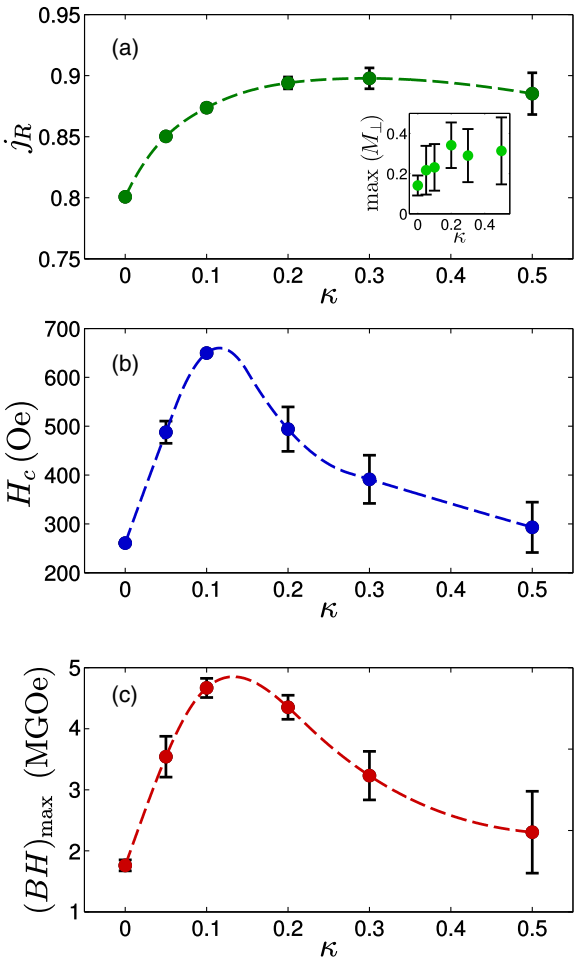

FIG. 5. (a) Remanence, (b) coercivity, and (c) energy product of a simulated nanocomposite $SrFe_{12}O_{19}/Fe$ with spherical hard grains as functions of exchange weakening on the grain boundaries. The inset in (a) represents the maximal value of the perpendicular (to the directions of the applied field) component of magnetization during the remagnetization process. The dashed lines are guides for the eye.

accessible for simulations. Otherwise, we might end up with a case where we are simulating the magnetization reversal of a system consisting of a single (or very few) cluster(s), so that the corresponding results will be nonrepresentative for the analysis of real experiments.

The best quantitative method to determine $\langle d_{\mathrm{cl}} \rangle$ is the calculation of the spatial correlation function of magnetization components perpendicular to the applied field (in our case, M_x and M_y): the average value of these components should be zero, and the decay length of their correlation functions, $C_x(\mathbf{r}) = \langle M_x(0) M_x(\mathbf{r}) \rangle$ (the same for M_y), would provide the most reliable estimation of $\langle d_{\mathrm{cl}} \rangle$.

However, taking into account a complex 3D character of $C_{x,y}(\mathbf{r})$, we adopt another criterion to determine the approximate number of independent clusters contained in our simulated system. Namely, as the figure of merit, we have employed the maximal value of the perpendicular

component of the total system magnetization $m_\perp = \sqrt{M_x^2 + M_y^2}/M_s$ during the magnetization reversal.

If the system contains only one (or very few) cluster(s), then, for some field during the reversal process, this component should be large (close to 1) because one cluster reverses in nearly the same fashion as a single particle, i.e., its magnetization rotates as a whole without significantly changing its magnitude. Hence, at a certain reversal stage, $m_\perp$ would unavoidably become relatively large. In the opposite case, where a system contains many nearly independent clusters ($N_{\rm cl} \gg 1$), their components $M_{x,i}$ and $M_{y,i}$ ($i = 1, \ldots, N$), being independent variables with zero mean, would average themselves out, leading to small values of $m_\perp$.

A simple statistical analysis based on the assumption of the independence of different clusters shows that the number of such clusters can be estimated as $N_{\rm cl} \geq 1/m_\perp^2$. This estimation means that we produce statistically significant results up to $m_\perp \approx 0.3$ because, in this case, $N_{\rm cl} \geq 10$. The corresponding analysis shows that, for our systems (containing about 5×10^5 finite elements), statistically significant results are produced up to $\kappa \approx 0.5$, so below we show results only in this range of exchange couplings.

The simulation results showing basic characteristics of the hysteresis loop—remanence j_R, coercivity H_c, and energy product $E_{\rm max} = (BH)_{\rm max}$—for the $SrFe_{12}O_{19}$/Fe composite as functions of the exchange weakening κ are presented in Fig. 5. We remind the reader that, for these simulations, approximately spherical hard grains are used.

From Fig. 5, it can be clearly seen that the remanence j_R of this material depends relatively weak on the intergrain exchange coupling. The reason is that j_R is very high already for the fully exchange-decoupled composite [$j_R(\kappa = 0) \approx 0.8$]. Such a high value, in turn, is due to the fact that the remanence is governed by the soft phase consisting of *cubical* grains. The remanence of the noninteracting (ideal) ensemble of such grains is $j_R^{(0)} \approx 0.83$. This high remanence cannot be significantly increased by the exchange interaction within the soft phase (as is the case for the system of *uniaxial* particles with randomly distributed anisotropy axes, where $j_R^{(0)} = 0.5$; see also Ref. [31] for an analysis of a corresponding 2D system). Neither can this remanence be substantially decreased by the exchange coupling with hard grains because their magnetization at $H_z = 0$ is still nearly aligned along the initial field direction due to the strong magnetizing field from the Fe soft phase (with its high magnetization $M_{\rm Fe} = 1700$ G).

In contrast to j_R, the coercivity H_c exhibits a pronounced maximum as the function of the exchange coupling κ, resulting in the corresponding maximum of the κ dependence of the maximal energy product $(BH)_{\rm max}(\kappa)$. We explain the reasons for the appearance of this maximum below, analyzing the hysteretic behavior of our nanocomposite for various κ's.

For the smallest nonzero κ studied here, the magnetization-reversal process is depicted in Fig. 6, where hysteresis loops for the soft and hard phases are shown separately and the magnetization configuration is displayed for several characteristic external fields. First, it can be clearly seen

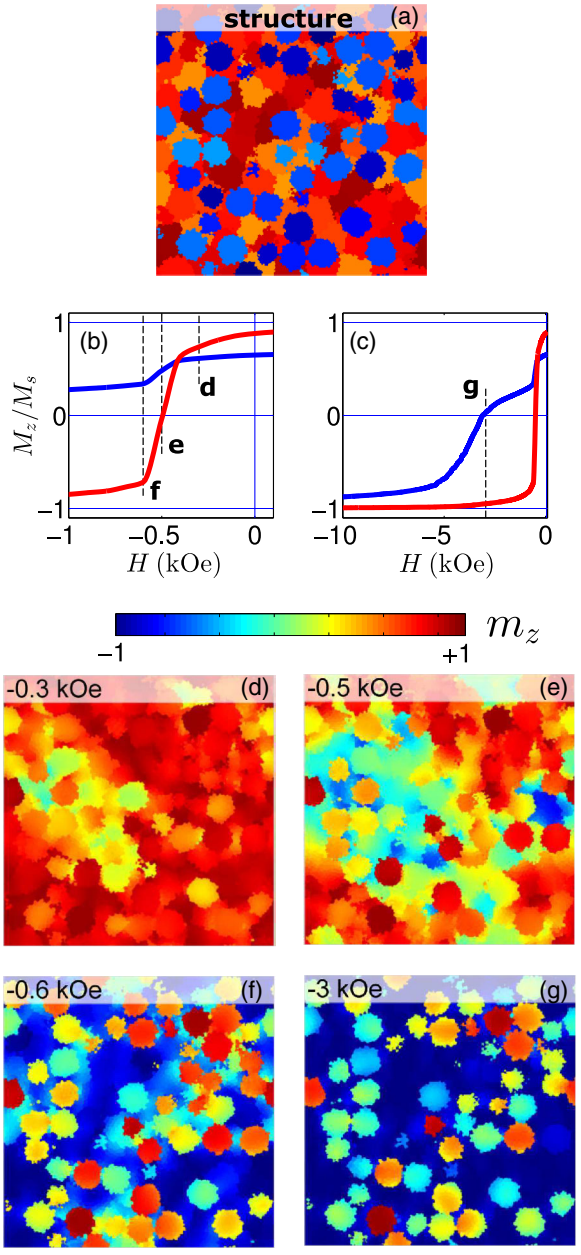

FIG. 6. Magnetization-reversal process for the composite with exchange weakening $\kappa = 0.05$. (Top to bottom) (a) Two-dimensional cut of the microstructure of the system (warm colors represent soft grains; cold colors represent hard grains). (b), (c) Hysteresis shown as separate curves for the soft (red lines) and hard (blue lines) phases (note the different scales of the H axis). (d),(e),(f),(g) Magnetization configurations shown as m_z maps for field values indicated on the hysteresis plots shown above.

that the magnetizations of the soft and hard phases reverse separately. An inspection of the magnetization configurations shows that the reversal of magnetic moments starts within the soft phase [see Fig. 6(d)] around the hard grains whose anisotropy axes are directed "favorably" (i.e., they deviate strongly from the initial field direction). Then the reversed area expands, occupying even larger regions of the soft phase [Fig. 6(e)] until nearly the entire soft phase is reversed [Fig. 6(f)]. Note that, in the negative field corresponding to this nearly complete reversal of the soft phase, the majority of the hard phase is still magnetized approximately along the initial direction. Only in much larger negative fields [Fig. 6(c)], the hard-phase magnetization also starts to reverse [Fig. 6(g)].

We emphasize here two important points: although the exchange coupling between the soft and hard phases is very weak ($\kappa = 0.05$) and the concentration of the hard phase is moderate (40%), the supporting action of the hard phase is enough to nearly double the coercivity of the soft phase—and hence of the whole system, when compared to the case of $\kappa = 0$ (see Fig. 5). At the same time, because of this low exchange coupling, hard grains reverse separately from the soft phase and nearly separately from each other [see Fig. 6(f)], leading to a high coercivity of the hard phase [Fig. 6(c)].

For the larger exchange coupling $\kappa = 0.1$ (see Fig. 7), the supporting effect of the hard phase increases the coercivity of the soft phase even further (compared to $\kappa = 0.05$). At the same time, this larger coupling also leads to the much earlier reversal of the hard phase, significantly decreasing its coercivity—see the hysteresis plots in Fig. 7. Magnetization reversal for this coupling starts in those system regions where the hard phase is nearly absent (due to local structural fluctuations)—see Fig. 7(e)—and is much more cooperative than for $\kappa = 0.05$.

The resulting coercivity of the entire system is at its maximum because the interphase coupling is, on the one hand, large enough to prevent the soft phase from a reversal in small fields, but, on another hand, small enough to enable a reversal of the hard phase in much higher negative fields than the soft phase.

When the intergrain exchange coupling is increased further, magnetization reversal of the system becomes fully cooperative, so the soft and hard phases reverse simultaneously (in the same negative fields)—see the hysteresis loops shown in Fig. 8 for $\kappa = 0.2$. Spatial correlations between the microstructure and the nucleation regions for the magnetization reversal become weak, as can be seen from microstructural and magnetic maps presented in this figure. It is also apparent that the correlation distance of the magnetization configuration strongly increases, as is noted in the discussion above.

The overall result is the decrease of the system coercivity because the soft phase causes a much earlier reversal of the hard phase, so the supporting effect of the high anisotropy

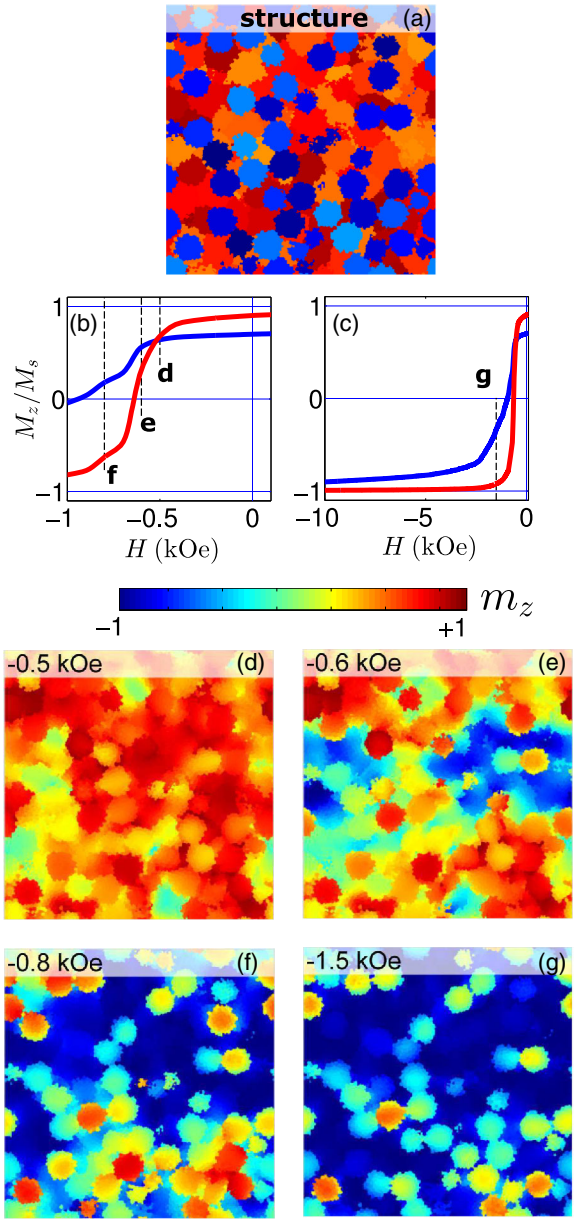

FIG. 7. Magnetization reversal for the composite with the exchange weakening $\kappa = 0.10$ presented in the same manner as in Fig. 6.

of the hard phase becomes smaller. However, for this relatively low value of $\kappa = 0.2$, this supporting effect is still present: $H_c(\kappa = 0.2)$ is nearly twice as large as $H_c(\kappa = 0)$.

When the exchange coupling increases even further, the magnetization reversal becomes completely dominated by the soft phase due to its larger magnetization and volume fraction. Specifically, for $\kappa = 0.5$, both the coercivity and the energy product are nearly the same as for $\kappa = 0$. We note that hysteresis loops for these two cases ($\kappa = 0$ and $\kappa = 0.5$) look qualitatively different, but this physically important difference (two-step vs one-step magnetization reversal) does not matter for the performance of the

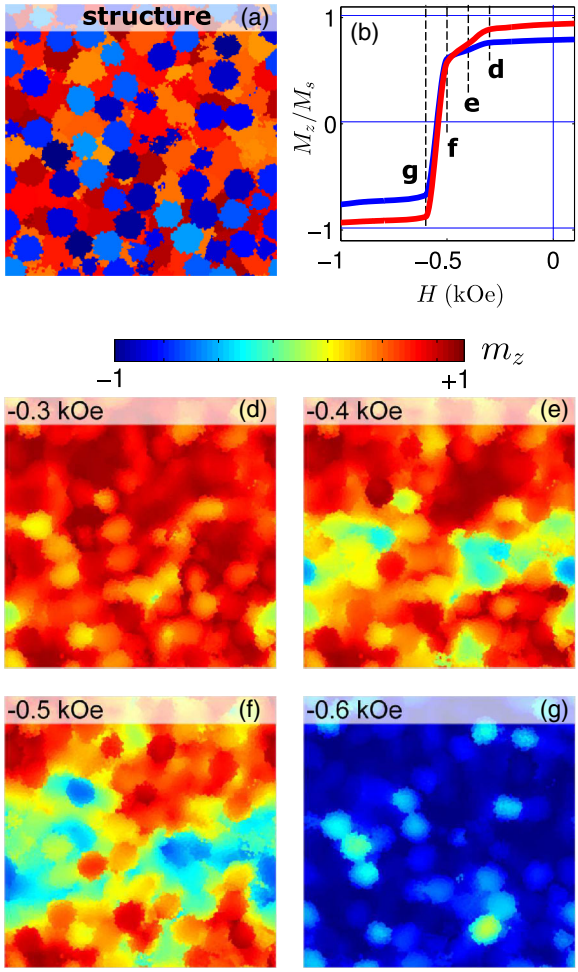

FIG. 8. Magnetization reversal for the composite with the exchange weakening $\kappa = 0.20$ presented in the same way as in Fig. 6. Simultaneous reversal of the hard and soft phases is clearly visible.

nanocomposite from the point of view of a material for permanent magnets.

The nonmonotonic dependence of the maximal energy product on the exchange coupling $(BH)_{\max}(\kappa)$ can be easily deduced from the dependencies $j_R(\kappa)$ and $H_c(\kappa)$. When κ increases from 0 to about 0.1, both the remanence and the coercivity increase, resulting in the rapid growth of $(BH)_{\max}$. For $\kappa > 0.1$, the small increase of the remanence (up to $\kappa \approx 0.2$) cannot compensate for the large drop of coercivity, resulting in an overall decrease of the energy product. We point out here that such a behavior occurs only when the dependence of the coercivity on the corresponding parameter (in our case, the exchange weakening κ) is really strong. The case where the coercivity depends relatively weakly on the parameter of interest is analyzed in detail in the next subsection.

In summary, we have shown that, in contrast to the common belief, there exists an *optimal* value of the interphase exchange coupling in a soft-hard nanocomposite which provides the maximal energy product. This optimal value obviously depends on the fractions of the soft and hard phases, but it is very likely that the optimal coupling should be significantly less than the perfect coupling ($\kappa = 1$) for all reasonable compositions in this class of materials.

This important insight opens up an alternate route for the optimization of the permanent-magnet materials.

B. Effect of the grain shape of the hard phase in $SrFe_{12}O_{19}/Fe$ and $SrFe_{12}O_{19}/Ni$ composites

One of the intensively discussed questions when optimizing the nanocomposite materials for permanent magnets is whether the materials containing the hard grains with the *nonspherical* shape could provide an improvement of the energy product for corresponding composites (see the corresponding references in the Introduction).

The standard argument in favor of the possible improvement of $E_{\max}$ is the additional shape anisotropy of nonspherical particles. For an elongated (prolate) ellipsoid of revolution, this anisotropy could increase the already-present magnetocrystalline anisotropy (MC anisotropy), thus enhancing the coercivity of the hard phase—and hence the energy product. Below, we will demonstrate that this line of arguments is not really conclusive and that the grain-shape effect may even be the opposite—the energy product can be larger for a material containing *oblate* hard grains.

Before proceeding with the analysis of our results, we emphasize that the *relative* contribution of the shape anisotropy can be approximately the same for rare-earth and ferrite-based materials. The former materials have a much larger MC anisotropy, $K_{\rm cr}$, so that, at first glance, shape effects for rare-earth hard grains should be much smaller. However, the relation between the shape anisotropy and the MC-anisotropy contributions is determined by not only the value of $K_{\rm cr}$ but also the reduced anisotropy constant $\beta = 2K_{\rm cr}/M_s^2$, which gives, roughly speaking, the relation between the MC-anisotropy energy and the self-demagnetizing energy of a particle.

The presence of the material magnetization in the denominator of the expression for β makes the constants for both material classes very similar. For example, the MC anisotropy $K_{\rm cr} \approx 4.6 \times 10^7$ erg/cm^3 for $Nd_2Fe_{14}B$ is more than one order of magnitude larger than its counterpart, $K_{\rm cr} \approx 4 \times 10^6$ erg/cm^3 for $SrFe_{12}O_{19}$. However, the much lower magnetization $M_s \approx 400$ G of $SrFe_{12}O_{19}$ compared to $M_s \approx 1300$ G of $Nd_2Fe_{14}B$ makes the difference between the reduced anisotropies of these materials quite small, $\beta_{\rm NdFeB} \approx 60$, whereas $\beta_{\rm SrFeO} \approx 50$.

In the language of the anisotropy field, we have to compare the values of the MC-anisotropy field $H_K = \beta M_s = 2K_{\rm cr}/M_s$ with the values of the *magnetizing* magnetodipolar field, which attains its maximal value $H_{\rm dip}^{\max} = 2\pi M_s$ for a needlelike particle. The corresponding relation $H_{\rm dip}^{\max}/H_K = \pi M_s^2/K_{\rm cr} = 2\pi/\beta$ is about 0.10 for $Nd_2Fe_{14}B$

and about 0.13 for $SrFe_{12}O_{19}$. This result indicates that, for the best case, the effect of the shape anisotropy for both material classes can achieve approximately 10%. We emphasize that even this moderate value would mean a non-negligible progress on a highly competing market of modern permanent-magnet materials.

Unfortunately, several circumstances are expected to strongly diminish the shape-anisotropy contribution. First, the estimate above holds for a strongly elongated particle; for ellipsoidal particles with a realistic aspect ratio, $a/b \sim 2$–3 (where a is the length of the axis of revolution), the shape anisotropy field is only about half of its maximal value. Second, this estimation holds for a single-domain particle, whereas strongly elongated or nearly flat particles acquire a multidomain state much easier than the spherical ones because the domain-wall energy for strongly nonspherical particles is much smaller than for a sphere. Finally, the relation derived above is true only for an isolated particle, and hard grains in nanocomposites are always embedded in a soft phase or are in close contact with other hard grains.

For these reasons, we perform a detailed numerical study of the dependence of hysteresis properties on the hard-grain shape for nanocomposite $SrFe_{12}O_{19}/Fe$ and—for comparison—for $SrFe_{12}O_{19}/Ni$. For this purpose, we simulate magnetization reversal in these composites with the hard grains having the shape of ellipsoids of revolution (spheroids) with the aspect ratio $a/b = 0.33$, 0.5, 1.0, 2.0, 3.0; aspect ratios $a/b > 1$ correspond, as usual, to prolate spheroids. For all aspect ratios, the volume of a single hard grain is kept the same (and equal to the volume of the approximately spherical grains with $D = 25$ nm). Volume concentration of the hard phase $c_{\text{hard}} = 40\%$ is the same as for the simulations reported in Sec. III A. The exchange-weakening parameter $\kappa = 0.1$ is chosen to be close to the optimal value for spherical hard grains obtained above.

1. *Grain-shape effect for* $SrFe_{12}O_{19}/Fe$

First, we discuss the simulation results obtained for the composite $SrFe_{12}O_{19}/Fe$—see Figs. 9, 10, and 11. In Fig. 9, magnetization-reversal curves for different aspect ratios of a/b are shown; both the loops for the entire system and for the soft and hard phases separately are presented. The most interesting observation here is the pronounced difference between the reversal curves of soft and hard phases for $a/b = 1$ and the nearly synchronous magnetization reversal of both phases for other aspect ratios shown in the figure. This observation is a key for the understanding of the system behavior that is discussed in detail now.

Overall dependencies of the basic hysteresis parameters j_R, H_c, and $(BH)_{\max}$ on the aspect ratio a/b are presented in Fig. 10. Both main parameters of the hysteresis—the remanence j_R and the coercivity H_c—exhibit a highly

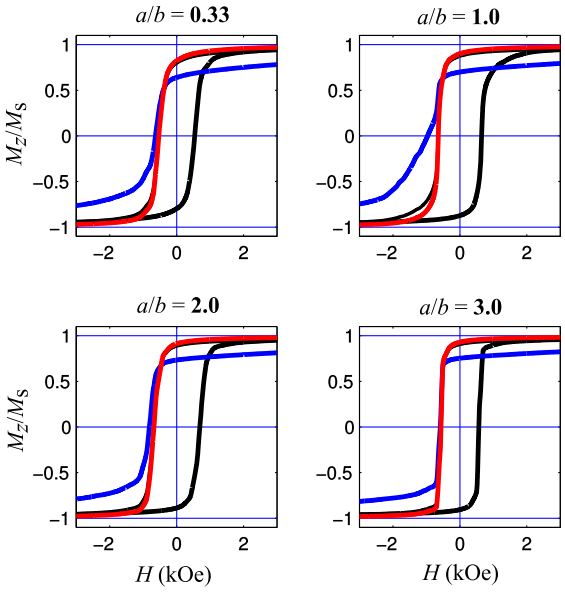

FIG. 9. Simulated hysteresis curves of the nanocomposite $SrFe_{12}O_{19}/Fe$ for the exchange weakening $\kappa = 0.1$ and for different aspect ratios of hard crystallites, as indicated in the panels. Black loops, the hysteresis of the total system; blue curves, the upper part of the hysteresis loop for the hard phase; red curve, the same for the soft phase.

nontrivial dependence on this aspect ratio, which should be carefully analyzed.

The dependence $j_R(a/b)$ shown in Fig. 10 is clearly counterintuitive because, normally, one would expect a *higher* remanence for a system containing elongated particles—in our case, for $a/b > 1$—due to the positive shape-anisotropy constant for such particles. The simulated dependence shows the opposite trend—the remanence increases with a decreasing aspect ratio a/b, i.e., j_R becomes *larger* for a composite with *oblate* hard grains.

This behavior can be explained by taking into account the fact that hard ellipsoidal grains are mostly embedded in the soft magnetic matrix (the soft phase), whose magnetization is larger than that of the hard phase: $M_{\text{Fe}} > M_{SrFe_{12}O_{19}}$. For this reason, hard grains represent magnetic "holes" inside a soft matrix (i.e., inclusions whose magnetization is smaller than the matrix magnetization). This observation means, in turn, that the total magnetodipolar field acting on the magnetization of the hard grain is directed (on average) towards the initially applied field. In other words, this field acts as a magnetizing field; i.e., it increases the remanence of the hard phase.

The magnitude of this magnetizing field is proportional to the difference between magnetizations of the soft and hard phases and is of the order $H_{\text{dip}}^{\text{mag}} \sim N_{\text{dem}} \cdot (M_{\text{Fe}} - M_{SrFe_{12}O_{19}}) = N_{\text{dem}} \Delta M$. For our system parameters, $\Delta M = 1300$ G, so that, taking into account that $N_{\text{dem}} \sim \pi$, we obtain $H_{\text{dip}}^{\text{mag}} \sim 4$ kOe. This value is comparable to the MC-anisotropy field of the hard grain itself

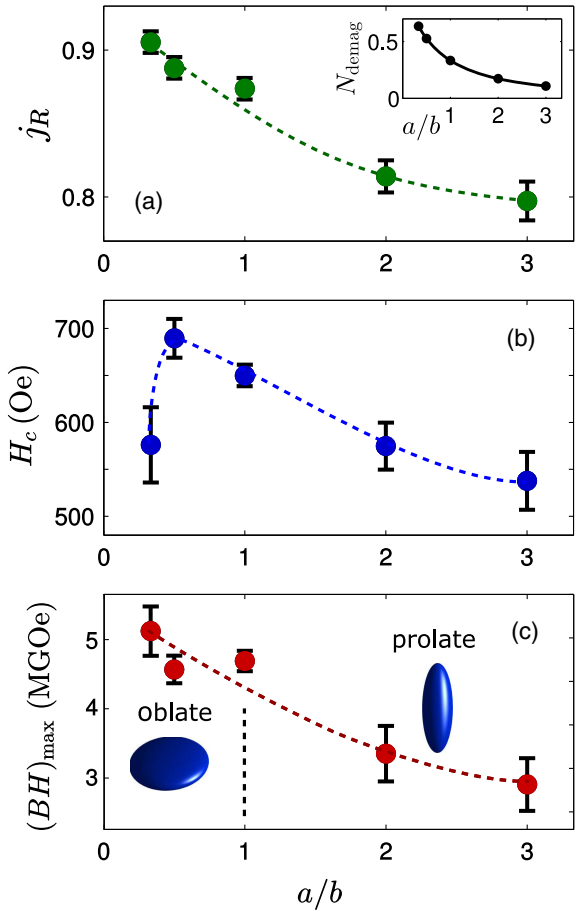

FIG. 10. (a) Simulated reduced remanence, (b) coercivity, and (c) energy product of the nanocomposite $SrFe_{12}O_{19}/Fe$ with different aspect ratios (a/b) of hard grains. The inset in (a) shows the demagnetizing factor, depending upon a/b. The dashed lines are guides for the eye.

$[H_K(SrFe_{12}O_{19}) = 20$ kOe], so the effect of this magnetodipolar field can be significant.

To explain the trend $[j_R(a/b)]$ seen in Fig. 10, it remains to note only that this magnetizing field is larger for oblate spheroids, for which it can achieve the magnitude of $4\pi\Delta M_s$—the limiting case for a thin disk with the revolution axes along the magnetizing direction of the system. By contrast, for the prolate spheroid, $H_{\rm dip}^{\rm mag}$ becomes weaker when a/b increases (the spheroid becomes more prolate) because the main contribution to this field comes from the soft-phase regions near the ends of this prolate spheroid.

The result of this complicated interplay is better alignment of the magnetic moments of the hard phase consisting of oblate particles. This improved alignment leads to higher remanence of the whole system, for two reasons: (i) the remanence of the hard phase itself is larger and (ii) the supporting action of the hard phase on the soft phase—due to the interphase exchange coupling—is more significant.

The explanation of the nontrivial dependence of the coercivity on the aspect ratio $H_c(a/b)$—with the maximum

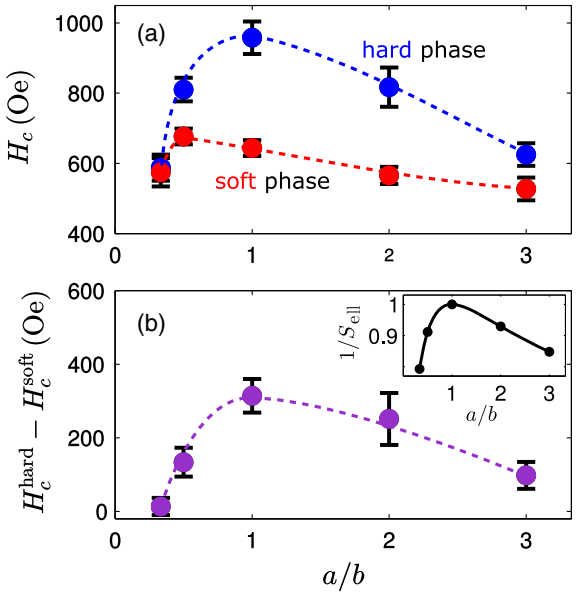

FIG. 11. (a) Coercivities of the hard, $H_c^{\rm hard}$ (blue circles), and soft, $H_c^{\rm soft}$ (red circles), phases and (b) the difference, ΔH_c, between these coercivities as functions of the aspect ratio a/b. [Inset of (b)] Inverse of the surface area of an ellipsoid of revolution, depending upon a/b. The dashed lines are guides for the eye. See the text for a detailed explanation.

between $a/b = 0.5$ and $a/b = 1.0$—requires a detailed understanding of the magnetization-reversal mechanism in composites with partial interphase exchange coupling.

Namely, magnetization reversal of these nanocomposites always occurs according to the following scenario: the soft phase switches first and then exhibits a torque on the hard grains due to the interphase exchange interaction. For a non-negligible interphase exchange, this torque is the main interaction mechanism between the phases and leads (together with the applied field) to the magnetization reversal of the hard phase in larger negative external fields.

In order to understand why the coercivity has its maximum for particles with a weak shape anisotropy, we have to recall that the interphase exchange interaction is a surface effect and, as such, is proportional to the interphase surface area. In our case, this interphase area is the surface area of hard grains, which are mostly surrounded by the soft phase. For this reason, the exchange torque which the soft phase exhibits on the hard grains is proportional to the surface area of these grains. Hence, this torque should be minimal for the hard grains with the spherical shape because the surface area of an ellipsoid of revolution with the given volume is minimal for $a/b = 1$ (a sphere).

For this reason, a hard phase with grains having a shape close to spherical has the maximal coercivity, i.e., reverses in the largest negative field. Such grains are also able to "support" a soft phase up to negative fields larger than nonspherical hard grains can, leading to the largest coercivity of the whole sample.

To provide further proof of this hypothesis, we plot in Fig. 11 the coercivities of the hard and soft phases separately [see the curves for H_c^{hard} and H_c^{soft} in Fig. 11(a)] and the difference between them, ΔH_c, in Fig. 11(b) as functions of the aspect ratio a/b. The excellent qualitative agreement between $\Delta H_c(a/b)$ and the inverse of the surface area of an ellipsoid of revolution $1/S_{\mathrm{ell}}(a/b)$ [see the Fig. 11(b) inset] as functions of a/b clearly shows that the observed effect is due to the surface-mediated interaction, which, in our case, clearly refers to the interphase exchange interaction.

We finish this subsection with an explanation for why the dependence of the maximal energy product on the aspect ratio $E_{\mathrm{max}}(a/b)$ [Fig. 10(c)] for our system closely follows the corresponding trend of the remanence $j_R(a/b)$ [see Fig. 10(a)], but it is not influenced by the dependence $H_c(a/b)$ [Fig. 10(b)].

To understand this phenomenon, we recall that the energy product is defined as the maximal value of the product (BH) within the second quadrant of the hysteresis loop, i.e., for external fields $-H_c < H < 0$ (here and below, we omit, for simplicity, the index z by H, B, and M):

$$E_{\mathrm{max}} = \max_{-H_c<H<0}[B(H)\cdot H] = \max\{[H+4\pi M(H)]\cdot H\}, \tag{2}$$

where it is important that the energy product depends on H—both explicitly and implicitly—via the dependence $M(H)$.

Let us now assume that, for some reference parameter value (e.g., in our case, for $a/b=1$) with the magnetization vs field dependence given by the function $M_{\mathrm{ref}}(H)$, the product (2) reaches its maximum $E_{\mathrm{max}}^{(0)}$ for the field value H_0. Then the corresponding derivative of the energy product dE/dH vanishes at this point, leading to the condition

$$\frac{d}{dH}\{[H+4\pi M_{\mathrm{ref}}(H)]\cdot H\}|_{H=H_0} = H_0 + 2\pi\left[M_{\mathrm{ref}}(H_0) + H_0\left.\frac{dM_{\mathrm{ref}}}{dH}\right|_{H=H_0}\right] = 0. \tag{3}$$

If the parameter in question changes (i.e., if we take another value of a/b), then the hysteresis loop also changes, becoming $M_{\mathrm{new}}(H) = M_{\mathrm{ref}}(H) + \Delta M$, and the maximum of the energy product is achieved at another field, $H_{\mathrm{new}} = H_0 + \Delta H$. The new maximal energy product then is

$$E_{\mathrm{max}}^{\mathrm{new}} = [H_{\mathrm{new}} + 4\pi M_{\mathrm{new}}(H_{\mathrm{new}})]\cdot H_{\mathrm{new}}. \tag{4}$$

Assuming that ΔM and ΔH are small, we can expand the functions $M_{\mathrm{ref}}(H)$ and $\Delta M(H)$ in the vicinity of the point H_0. Starting with Eq. (4) and retaining only terms that are linear in ΔM and ΔH, we obtain for $E_{\mathrm{max}}^{\mathrm{new}}$ the expression

$$E_{\mathrm{max}}^{\mathrm{new}} = E_{\mathrm{max}}^{(0)} + 4\pi H_0\Delta M(H_0) + 2\Delta H\left\{H_0 + 2\pi\left[M_{\mathrm{ref}}(H_0) + H_0\left.\frac{dM_{\mathrm{ref}}}{dH}\right|_{H=H_0}\right]\right\}. \tag{5}$$

The coefficient in the curly braces after ΔH is precisely the expression (3) at the point where the reference energy product reaches its maximum and, as such, is equal to zero. Hence, we are left with the following expression of the new maximal energy product:

$$E_{\mathrm{max}}^{\mathrm{new}} = E_{\mathrm{max}}^{(0)} + 4\pi H_0\Delta M(H_0). \tag{6}$$

This expression shows that the change of the energy product due to the variation of some external system parameter is controlled mainly by the change of the magnetization curve (the upper part of the M-H hysteresis loop) at the external field H_0, where the reference energy product reaches its maximum. Obviously, this magnetization change is roughly proportional to the remanence change, which explains the semiquantitative correspondence between the dependencies $j_R(a/b)$ and $E_{\mathrm{max}}(a/b)$. We point out once more that this statement is true only if the coercivity shift due to the variation of this parameter is relatively small. If this shift is not small, then the position of the vertical side of the rectangle [in the $(B$-$H)$ plane] used for the determination of $(BH)_{\mathrm{max}}$ can strongly depend on the coercivity value, making the derivation of Eq. (5) invalid.

2. *Grain-shape effect for* $SrFe_{12}O_{19}/Ni$

The second composite which we have used to study the grain-shape effect—$SrFe_{12}O_{19}/Ni$—is qualitatively different from the previous material ($SrFe_{12}O_{19}/Fe$) due to the much lower magnetization of the soft phase: $M_s(\mathrm{Ni}) \approx 490$ G. The idea behind the usage of a soft phase with such a low magnetization is that the coercivity of the resulting material should be much higher due to the weaker response of the soft phase, with a smaller magnetization to the external field. This higher coercivity might compensate for the decrease of the net magnetization, resulting in a competitive energy product.

Simulation results for $SrFe_{12}O_{19}/Ni$ with various grain shapes are presented in Fig. 12 (the hysteresis loops) and Fig. 13 (the basic characteristics of the hysteresis). As can be clearly seen, the Ni-containing composite behaves qualitatively differently than the Fe-containing material.

The main new feature is—as expected—the higher coercivity of both the soft and hard phases. The considerably larger coercivity of the Ni phase [$H_c(\mathrm{Ni}) \approx 1000$ Oe—see Fig. 12, the red loops] compared to the coercivity of the Fe phase in the previously studied

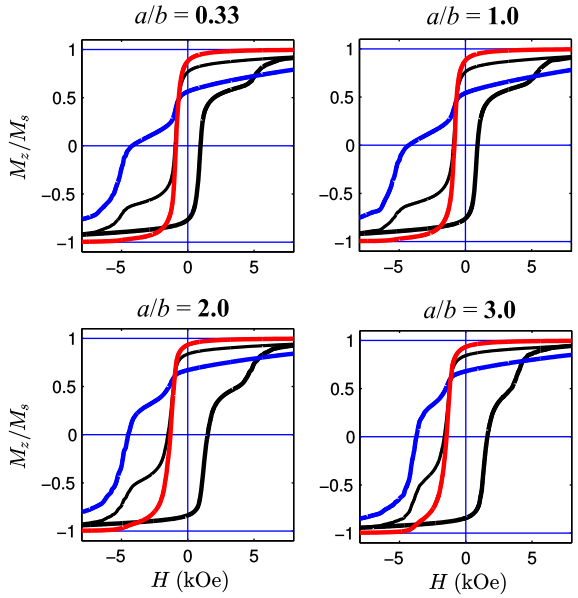

FIG. 12. Simulated hysteresis curves of the composite $SrFe_{12}O_{19}/Ni$ for $\kappa = 0.1$ and different aspect ratios of hard crystallites, as indicated in the panels. Black loops are total hysteresis; blue curves represent upper part of the hysteresis loops for the hard phase; red curves represent upper part of the hysteresis loops for the soft phase.

composite [$H_c(\mathrm{Fe}) \approx 600$ Oe—see Fig. 11(a)] is mainly due to the lower magnetization of Ni, as mentioned above.

The much larger coercivity of the hard phase (we remind the reader that this phase is the same for both of the studied materials) for $SrFe_{12}O_{19}/Ni$ can most probably be explained by three reasons. First, due to the lower value of $M_s(\mathrm{Ni})$, the reversal of the soft phase starts for the Ni-containing composite in higher negative fields, which in itself should lead to a larger H_c^{hard} for the hard phase also. However, this reason alone could not be responsible for the more than fourfold increase of H_c^{hard} [$H_c^{\mathrm{hard}}(SrFe_{12}O_{19}/Ni) \approx 4000$ Oe vs $H_c^{\mathrm{hard}}(SrFe_{12}O_{19}/Fe) < 1000$ Oe].

The second reason is that the magnetodipolar field of the soft phase acting on hard grains is much smaller for Ni- than for Fe-containing composites (due to the same much lower magnetization of Ni). After the reversal of the soft phase, this magnetodipolar field is directed oppositely to the initial material saturation and thus assists the reversal of hard grains. The much smaller magnitude of this field thus leads to a much higher external field required to reverse the hard phase.

Finally, the considerably smaller exchange constant of Ni compared to Fe (see Table I) results in the lower exchange torque acting on hard grains after the reversal of the soft phase, also decreasing the total torque acting on the hard phase and increasing its coercivity.

This qualitatively new situation—the noncorrelated magnetization reversals of the soft and hard phases—leads to another type of coercivity dependence on the aspect ratio

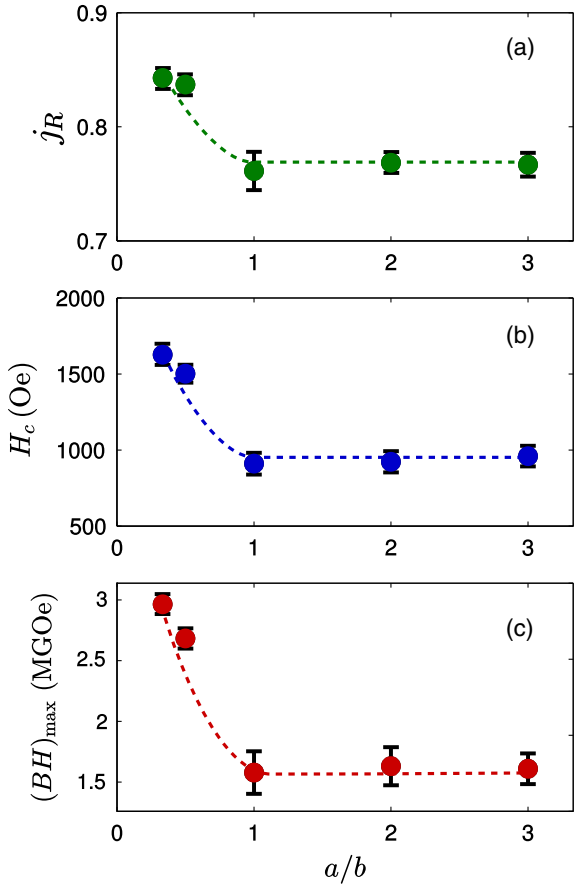

FIG. 13. (a) Remanence, (b) coercivity, and (c) energy product of the nanocomposite $SrFe_{12}O_{19}/Ni$, depending upon the aspect ratio a/b of the hard grains. The dashed lines are guides for the eye.

a/b of hard grains: coercivity $H_c(a/b)$ decreases when this ratio increases [see Fig. 13(b)], behaving in a manner very similar to the remanence $j_R(a/b)$ [Fig. 13(a)].

The most likely explanation for this behavior is the following: the degree of the magnetization alignment of hard grains is nearly the same for various aspect ratios a/b. Hence, the main effect on the soft-phase reversal is due to the difference in the magnetodipolar-field distributions caused by hard grains having various shapes. Prolate ellipsoids of revolution produce a nonuniform magnetodipolar field whose maximal value is higher than for oblate ellipsoids. However, the field of prolate particles is strongly concentrated near their "sharp" ends, whereas the dipolar field of oblate ellipsoids (magnetized, on average, along their axes of revolution) occupies a much larger region near their "flat" surfaces. For this reason, the dipolar field of oblate hard grains supports the magnetization of the soft phase in larger space regions, thus leading to an increase of the soft phase (and total) coercivity with a decreasing a/b, i.e., when hard grains become more oblate.

As the result of the decrease of both j_R and H_c, the energy product also decreases with an increasing a/b, as

shown in Fig. 13(c). We point out that, although the resulting behavior is qualitatively somewhat similar to the case of the Fe-containing material (compare to Fig. 10)—the energy product decreases with an increasing aspect ratio—the physical reasons for this behavior are fundamentally different for these two composites. In the two cases considered in this paper, the two mechanisms can be clearly differentiated. For the Fe-based composite, the coercivity change with a/b is relatively small (about 25%), so the energy product follows the dependence $j_R(a/b)$—see Eqs. (2)–(6)—and the first mechanism (the effect of the magnetizing field inside the hard grains) is at work. For the Ni-based system, the coercivity decrease with an increasing a/b is very large (more than 2 times), so the theory based on Eqs. (2)–(6) is not applicable. In this case, the energy product essentially follows the coercivity dependence $H_c(a/b)$, which is, as discussed above, most probably due to the change of the supporting influence of hard grains on the soft phase (the second mechanism).

It is also interesting to note that, despite the larger coercivity of the Ni-containing composite, its energy product remains smaller than for the Fe-containing material due to its much lower net magnetization. This relation can change for materials with different fractions of soft and hard phases.

IV. CONCLUSION

In this paper, we present a detailed numerical study for the dependence of magnetic properties of Sr-ferrite-based nanocomposites on two very important material parameters: (i) exchange coupling between various crystallites (which includes the coupling between soft and hard grains) and (ii) the shape of the hard grains.

First, we demonstrate—in contrast to the common paradigm—that the maximal energy product $E_{\max} = (BH)_{\max}$ is a nonmonotonic function of the intergrain exchange coupling κ and that the optimal κ value (for which the energy product reaches its highest value) is far below the perfect coupling. This nonmonotonic character of the function $E_{\max}(\kappa)$ is due to the corresponding dependence of the coercivity on the exchange coupling $H_c(\kappa)$.

Second, we studied the dependence of the hysteresis properties and the maximal energy product on the shape of hard grains for two very different nanocomposite materials —$SrFe_{12}O_{19}$/Fe [M_s(Fe) ≈ 1700 G] and $SrFe_{12}O_{19}$/Ni [M_s(Ni) ≈ 490 G]. Hard grains have been assumed to have (approximately) a shape of ellipsoids of revolution, whose aspect ratio is varied in the range $1/3 \le a/b \le 3$ ($a/b > 1$ corresponds to a prolate ellipsoid). We show that, for both materials, the aspect-ratio dependence of the maximal energy product $E_{\max}(a/b)$ essentially follows the corresponding dependence of the hysteresis-loop remanence $j_R(a/b)$ and support this observation with analytical considerations. For both materials, the maximal value of $j_R(a/b)$—and hence of $E_{\max}(a/b)$—is obtained for the oblate hard grains with the smallest aspect ratio, $a/b = 1/3$ (also, in contrast to common expectations). Physical reasons for this behavior are revealed.

Finally, we also analyze the dependence of the coercivity on the shape of the hard grains $H_c(a/b)$ and show that this dependence for the two composites under study is qualitatively different. For $SrFe_{12}O_{19}$/Fe, the function $H_c(a/b)$ has a pronounced maximum for approximately spherical grains, whereas, for $SrFe_{12}O_{19}$/Ni, coercivity monotonically decreases with an increasing a/b. This difference is explained by analyzing the dominating interaction mechanisms between the hard and soft phases in these materials.

ACKNOWLEDGMENTS

Financial support of the Deutsche Forschungsgemeinshaft under the Project No. BE2464/10-3 and the European Union's Seventh Framework Programme under the project "NANOPYME" (No. 310516) is greatly acknowledged. Also, we would like to thank Dr. Alberto Bollero, Dr. Adrián Quesada, and Dr. Cesar de Julian Fernandez for the fruitful discussions and Dr. Andreas Michels for his critical reading of the manuscript.

[1] R. L. Stamps, S. Breitkreutz, J. Åkerman, A. V. Chumak, Y. Otani, G. E. W. Bauer, J. Thiele, M. Bowen, S. Majetich, M. Kläui, I. Prejbeanu, B. Dieny, N. Dempsey, and B. Hillebrands, The 2014 magnetism roadmap, J. Phys. D **47**, 333001 (2014).

[2] O. Gutfleisch, Controlling the properties of high energy density permanent magnetic materials by different processing routes, J. Phys. D **33**, R157 (2000).

[3] J. M. D. Coey, *Magnetism and Magnetic Materials* (Cambridge University Press, Cambridge, England, 2010).

[4] R. Skomski, P. Manchanda, P. K. Kumar, B. Balamurugan, A. Kashyap, and D. J. Sellmyer, Predicting the future of permanent-magnet materials, IEEE Trans. Magn. **49**, 3215 (2013).

[5] Y. Matsuura, J. Hoshijima, and R. Ishii, Materials relation between $Nd_2Fe_{14}B$ grain alignment and coercive force decrease ratio in NdFeB sintered magnets, J. Magn. Magn. Mater. **336**, 88 (2013).

[6] R. Grössinger, G. Badurek, J. Fidler, M. Zehetbauer, and C. D. Dewhurst, Structural methods for studying nanocrystalline materials, J. Magn. Magn. Mater. **294**, 152 (2005).

[7] J. Liu, H. Sepehri-Amin, T. Ohkubo, K. Hioki, A. Hattori, T. Schrefl, and K. Hono, Effect of Nd content on the microstructure and coercivity of hot-deformed Nd-Fe-B permanent magnets, Acta Mater. **61**, 5387 (2013).

[8] H. Sepehri-Amin, T. Ohkubo, S. Nagashima, M. Yano, T. Shoji, A. Kato, T. Schrefl, and K. Hono, High-coercivity ultrafine-grained anisotropic Nd-Fe-B magnets processed by hot deformation and the Nd-Cu grain boundary diffusion process, Acta Mater. **61**, 6622 (2013).

[9] J. F. Löffler, H. B. Braun, W. Wagner, G. Kostorz, and A. Wiedenmann, Magnetization processes in nanostructured

metals and small-angle neutron scattering, Phys. Rev. B **71**, 134410 (2005).

[10] F. Y. Ogrin, S. L. Lee, M. Wismayer, T. Thomson, C. D. Dewhurst, R. Cubitt, and S. M. Weekes, Micromagnetic simulation of small-angle neutron scattering from magnetic recording media, J. Appl. Phys. **99**, 08G912 (2006).

[11] S. Erokhin, D. Berkov, N. Gorn, and A. Michels, Micromagnetic modeling and small-angle neutron scattering characterization of magnetic nanocomposites, Phys. Rev. B **85**, 024410 (2012).

[12] S. Erokhin, D. Berkov, N. Gorn, and A. Michels, Magnetic neutron scattering on nanocomposites: Decrypting cross-section images using micromagnetic simulations, Phys. Rev. B **85**, 134418 (2012).

[13] A. Michels, S. Erokhin, D. Berkov, and N. Gorn, Micromagnetic simulation of magnetic small-angle neutron scattering from two-phase nanocomposites, J. Magn. Magn. Mater. **350**, 55 (2014).

[14] Y. Gao, D. Shindo, and A. K. Petford-Long, Nonuniform magnetic structure in $Nd_2Fe_{14}B/Fe_3B$ nanocomposite materials, J. Appl. Phys. **93**, 8119 (2003).

[15] N. M. Saiden, T. Schrefl, H. A. Davies, and G. Hrkac, Micromagnetic finite element simulation of nanocrystalline α-$Fe/Nd_2Fe_{14}B/Fe_3B$ magnets, J. Magn. Magn. Mater. **365**, 45 (2014).

[16] M. Yi, O. Gutfleisch, and B.-X. Xu, Micromagnetic simulations on the grain shape effect in Nd-Fe-B magnets, J. Appl. Phys. **120**, 033903 (2016).

[17] C. B. Rong, H. W. Zhang, R. J. Chen, S. L. He, and B. G. Shen, The role of dipolar interaction in nanocomposite permanent magnets, J. Magn. Magn. Mater. **302**, 126 (2006).

[18] B. Zheng, H. W. Zhang, S. F. Zhao, J. L. Chen, and G. H. Wu, The physical origin of open recoil loops in nanocrystalline permanent magnets, Appl. Phys. Lett. **93**, 9 (2008).

[19] S.-l. He, H.-W. Zhang, C.-B. Rong, J. Chen, J.-R. Sun, and B.-G. Shen, Investigation on magnetic properties of orientated nanocomposite $Pr_2Fe_{14}B/\alpha$-Fe permanent magnets by micromagnetic finite-element method, J. Magn. Magn. Mater. **324**, 3853 (2012).

[20] R.-J. Chen, H. W. Zhang, C.-B. Rong, J.-R. Sun, and B. G. Shen, Micromagnetic simulation of angular dependence of coercivity in $Sm(Co, Fe, Cu, Zr)_z$ magnets, J. Appl. Phys. **100**, 043901 (2006).

[21] Y. Li, M. Yue, T. Wang, Q. Wu, D. Zhang, and Y. Gao, Investigation of magnetic properties of MnBi/Co and $MnBi/Fe_{65}Co_{35}$ nanocomposite permanent magnets by micro-magnetic simulation, J. Magn. Magn. Mater. **393**, 484 (2015).

[22] A. Donev, S. Torquato, and F. H. Stillinger, Neighbor list collision-driven molecular dynamics simulation for non-spherical hard particles, J. Comput. Phys. **202**, 765 (2005).

[23] L. Landau and E. Lifshitz, On the theory of the dispersion of magnetic permeability in ferromagnetic bodies, Phys. Zeitsch. Der Sow. **8**, 153 (1935).

[24] H. Kronmüller and S. Parkin, in *Handbook of Magnetism and Advanced Magnetic Materials, Vol. 2: Micromagnetism*, edited by H. Kronmüller and S. Parkin (Wiley, Chichester, England, 2007).

[25] A. Quesada, C. Granados-Miralles, A. López-Ortega, S. Erokhin, E. Lottini, J. Pedrosa, A. Bollero, A. M. Aragón, F. Rubio-Marcos, M. Stingaciu, G. Bertoni, C. de Julián Fernández, C. Sangregorio, J. F. Fernández, D. Berkov, and M. Christensen, Energy product enhancement in imperfectly exchange-coupled nanocomposite magnets, Adv. Electron. Mater. **2**, 1500365 (2016).

[26] N. Usov and S. Peschany, Theoretical hysteresis loops for single-domain particles with cubic anisotropy, J. Magn. Magn. Mater. **174**, 247 (1997).

[27] J. Garca-Otero, M. Porto, and J. Rivas, Henkel plots of single-domain ferromagnetic particles, J. Appl. Phys. **87**, 7376 (2000).

[28] D. Berkov, Numerical simulations of quasistatic remagnetization processes in fine magnetic particle systems, J. Magn. Magn. Mater. **161**, 337 (1996).

[29] E. C. Stoner and E. P. Wohlfarth, A mechanism of magnetic hysteresis in heterogeneous alloys, Phil. Trans. R. Soc. A **240**, 599 (1948).

[30] D. V. Berkov and S. V. Meshkov, Theory of remagnetization curves of dilute random magnets, JETP **67**, 2255 (1988).

[31] D. V. Berkov and N. L. Gorn, Quasistatic remagnetization processes in two-dimensional systems with random on-site anisotropy and dipolar interaction: Numerical simulations, Phys. Rev. B **57**, 14332 (1998).